JUSTC

Article

http://justc.ustc.edu.cn

Received: April 20, 2021; Accepted: November 26, 2021

# Sound speed imaging of small animal organs by ultrasound computed tomography

Zhiming Hu[1,2], Mingchun Yang[1,2], Xiang Zhu[1,2], and Chao Tian[1,2] ✉

[1]*Department of Precision Machinery and Precision Instrumentation, University of Science and Technology of China, Hefei 230027, China;*
[2]*Key Laboratory of Precision Scientific Instrumentation of Anhui Higher Education Institutes, University of Science and Technology of China, Hefei 230027, China*

✉Correspondence: Chao Tian, E-mail: ctian@ustc.edu.cn

## Graphical abstract

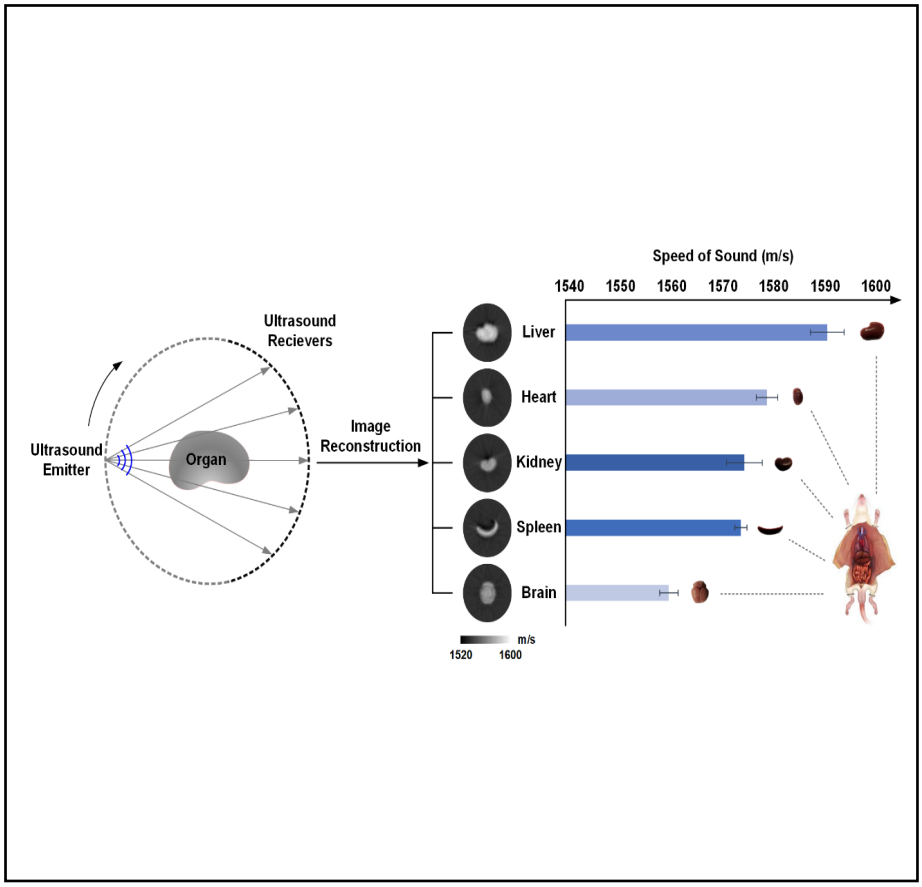


*Sound speed imaging of small animal organs by ultrasound computed tomography*

## Public summary

■ An ultrasound computed tomography system with a 256-element ring array transducer was developed for sound speed imaging and evaluation of small animal organs.

■ Sound speeds of five excised rat organs were imaged and measured and the results are consistent to published data.

■ This work demonstrates a new method for sound speed imaging and holds potential for in vivo applications.

**Citation:** Hu Z M, Yang M C, Zhu X, et al. Sound speed imaging of small animal organs by ultrasound computed tomography. *JUSTC*, **2022**, 52(1): 8. DOI: 10.52396/JUSTC-2021-0113

JUSTC

Article

http://justc.ustc.edu.cn

Received: April 20, 2021; Accepted: November 26, 2021

# Sound speed imaging of small animal organs by ultrasound computed tomography

Zhiming Hu[1,2], Mingchun Yang[1,2], Xiang Zhu[1,2], and Chao Tian[1,2] ✉

[1]*Department of Precision Machinery and Precision Instrumentation, University of Science and Technology of China, Hefei 230027, China;*
[2]*Key Laboratory of Precision Scientific Instrumentation of Anhui Higher Education Institutes, University of Science and Technology of China, Hefei 230027, China*

✉Correspondence: Chao Tian, E-mail: ctian@ustc.edu.cn

Cite This: *JUSTC*, **2022**, 52(1): 8 (6pp)  Read Online  SI Supporting Information

**Abstract:** Sound speed is an important acoustic parameter for tissue characterization. Herein we developed an ultrasound computed tomography (USCT) system for *ex vivo* sound speed imaging and evaluation of small animal organs. The proposed USCT system employs a 256-element ring array transducer and allows simultaneous signal transmission and reception for all channels. The method does not require complicated sample preparation procedures and can yield accurate measurement results. Experimental results show that sound speeds of excised rat brain, heart, liver, spleen, and kidney measured by the method are close to published data. This work demonstrates a new method for sound speed imaging and holds potential for *in vivo* applications.

**Keywords:** ultrasound computed tomography; sound speed; tissue characterization; image reconstruction

**CLC number:** TP18  **Document code:** A

## 1 Introduction

Sound speed ($c$) is an important acoustic parameter of biological tissues. It relates to two fundamental tissue properties, the elasticity ($K$) and the density ($\rho$) through the formula $c = (K/\rho)^{1/2}$. Since elasticity and density usually change with tissue state, the value of sound speed is helpful to reflect the pathophysiological condition of tissues and can be used as an important measure for disease diagnosis[1−5]. In particular, tissues with a high protein content usually have a higher sound speed while tissues (e.g. fat) with a high lipid content have a lower sound speed. Bamber and Hill showed that normal human livers have an average sound speed of 1577 $m\cdot s^{-1}$ while fatty livers have an average value of 1553 $m\cdot s^{-1}$[6]. It is also clear that cancerous breast tissue has an average sound speed of 1559 $m\cdot s^{-1}$ and is different from that in surrounding fat (≈ 1470 $m\cdot s^{-1}$) and glandular tissues (≈ 1515 $m\cdot s^{-1}$)[7]. Based on these facts, there are several groups worldwide working to map the sound speed distribution of breast tissues for noninvasive early cancer diagnosis[7−9].

In addition to probing the pathophysiological state of tissues, sound speed information is also important for image formation. In conventional ultrasound and photoacoustic imaging, soft tissue is usually assumed to be homogeneous and a constant sound speed is used for image reconstruction. However, actual biological tissues are heterogeneous and the sound speed in soft tissues varies significantly, which may yield substantial image distortion and artifacts and lead to degraded image contrast and resolution[10−13]. Accurate mapping of the sound speed of biological tissues is important for high-quality ultrasound and photoacoustic imaging.

Current sound speed measurement methods can be mainly divided into two groups, i.e., average sound speed estimation and local sound speed estimation. The average methods, such as beam tracking[14], transaxial compression[15] and phase variance[16], estimate the average sound speed between a transducer and its focal depth. These methods can produce accurate measurement results for homogenous media but may yield significant errors for *in vivo* measurements due to tissue heterogeneity[17]. The local sound speed estimation methods, such as the model-based method[17], the crossed-beam method[18] and the registered virtual detector method[19] are based on the pulse-echo principle and estimate sound speed in a localized target area[20]. These methods can provide improved sound speed measurement accuracy in a local area when tissue heterogeneities are present but they are not able to visualize entire sound speed maps of biological tissues. Compared with these methods, scanning acoustic microscopy can realize sound speed map imaging but needs special sample preparation procedures[21], which is not suitable for *in vivo* measurements.

Ultrasound computed tomography (USCT), first proposed by Greenleaf et al.[22] is a technique that works similarly as X-ray computed tomography and can produce accurate sound speed maps of soft tissues. USCT typically employs an array transducer, which consists of hundreds to thousands of elements. During imaging, one element of the array emits ultrasonic signals while the facing elements receive the signals. By repeating this process for each element and extracting the travel time of the signals from the emitters to the receivers, a sound speed tomogram can be reconstructed using geometrical acoustics or full-wave inversion based methods[7, 23]. Based on this principle, Rajagopalan et al studied the dependence of sound speed with temperature in various excised human tissues in 1979[24]. However, limited by transducer technology, electronics, and computing power, they only used a pair of



DOI: 10.52396/JUSTC-2021-0113
*JUSTC*, **2022**, 52(1): 8

transducers to perform the measurements. The imaging process was slow and the image quality needs improvement.

The objective of this study is to perform *ex vivo* imaging of the sound speed distribution of different organs and tissues of small animals using state-of-the-art USCT technology and provide reference data of sound speed for the medical ultrasound community. Towards this goal, we developed an advanced USCT system using a full ring array transducer and imaged the sound speed maps of different types of organs of normal rats, including the brain, heart, liver, spleen, and kidney. Average sound speed values were calculated and compared with published data.

## 2 Method

The USCT system developed to image the sound speed map of isolated organs and tissues is shown in Fig.1a. The system consists of the following parts: A water bath, a custom ring array ultrasound transducer, a research ultrasound platform, and a host computer. The water bath is filled with an ultrasound coupling medium and is equipped with a temperature controller, which can maintain the temperature of the coupling medium at 37 ± 0.2 ℃ for tissue imaging. The coupling medium used in this study is either water for gelatin phantom imaging or phosphate-buffered saline (PBS) for tissue imaging, whose acoustic properties have been well studied[25, 26]. The ring transducer array (diameter: 50 mm; center frequency: 3 MHz; element number: 256; Guangzhou Doppler Ltd., Guangzhou, China) is immersed in the water bath and is connected with the research ultrasound platform (Vantage 256, Verasonics Inc., WA, USA). The research ultrasound platform can perform real-time multichannel ultrasound transmission and reception through the ring array transducer and transfers received radiofrequency data to the host computer for image reconstruction.

The height $h$ and width $w$ of each transducer element are 10 mm and 0.5 mm, respectively. The near field distance $d$ is thus estimated to be 50 mm in the elevational plane according to the near field distance formula $d = h^2/4\lambda$, where $\lambda$ is the ultrasound wavelength. This indicates that the entire imaging region enclosed by the ring transducer array is within the near field region. Since the acoustic field in the near field region depends on the size of the transducer element, the elevational thickness of ultrasound beam used for sound speed imaging is approximately 10 mm. This value determines the elevational size of the tissue that is considered in the sound speed measurement.

The image reconstruction process works as follows. The travel time of ultrasound signals from the emitters to the receivers are first calculated by extracting the first arrival time of the received radiofrequency data using the Akaike information criterion (AIC)[27]. Based on the estimated travel time data, sound speed maps are reconstructed using the algebraic iterative algorithm with Laplacian regularization[28]. In this reconstruction algorithm, ultrasound is modeled as bent rays and the ROI is divided into discrete grids, as shown in Fig.1 b. As such, the bent rays traveling through the ROI can be mathematically represented by a series of linear equations as

$$\left.\begin{aligned} &a_{11}s_1 + a_{12}s_2 + \cdots + a_{1m}s_m = p_1 \\ &a_{21}s_1 + a_{22}s_2 + \cdots + a_{2m}s_m = p_2 \\ &\vdots \\ &a_{n1}s_1 + a_{n2}s_2 + \cdots + a_{nm}s_m = p_n \end{aligned}\right\} \tag{1}$$

where $a$ and $s$ denote the weight of the ray in the grid and the slowness (the reciprocal of sound speed) of sound in the grid, respectively; $p$ denotes the travel time of the ray from the emitter to the receiver; $m$ and $n$ represent the total number of grids and rays, respectively. Eq. (1) can be written in the matrix form as

$$\boldsymbol{A}\boldsymbol{s} = \boldsymbol{p} \tag{2}$$

where $\boldsymbol{A}$ is the coefficient matrix; $\boldsymbol{s}$ and $\boldsymbol{p}$ are the slowness vector and the projection vector, respectively. The matrix $\boldsymbol{A}$ and the vectors $\boldsymbol{s}$ and $\boldsymbol{p}$ can be written as

$$\boldsymbol{A} = \begin{bmatrix} a_{11} & a_{12} & \cdots & a_{1m} \\ a_{21} & a_{22} & \cdots & a_{2m} \\ \vdots & \vdots & \ddots & \vdots \\ a_{n1} & a_{n2} & \cdots & a_{nm} \end{bmatrix}, \boldsymbol{s} = \begin{bmatrix} s_1 \\ s_2 \\ \vdots \\ s_m \end{bmatrix}, \boldsymbol{p} = \begin{bmatrix} p_1 \\ p_2 \\ \vdots \\ p_m \end{bmatrix} \tag{3}$$

Based on this matrix equation, an objective function can be constructed as

$$U(\boldsymbol{s}) = \|\boldsymbol{A}\boldsymbol{s} - \boldsymbol{p}\|_2^2 + \|\mu\boldsymbol{L}\boldsymbol{s}\|_2^2 \tag{4}$$

where $\boldsymbol{L}$ is the Laplacian matrix and $\mu$ is a regularization coefficient. The second term in Eq. (4) denotes the Laplacian regularization to avoid possible numerical instability. Solving Eq. (2) is equivalent to minimize the functional $U(\boldsymbol{s})$ in Eq. (4) with respect to the slowness $\boldsymbol{s}$, which can be computed using the conjugate gradient least squares algorithm[29]. The final sound speed is calculated by averaging segmented sound

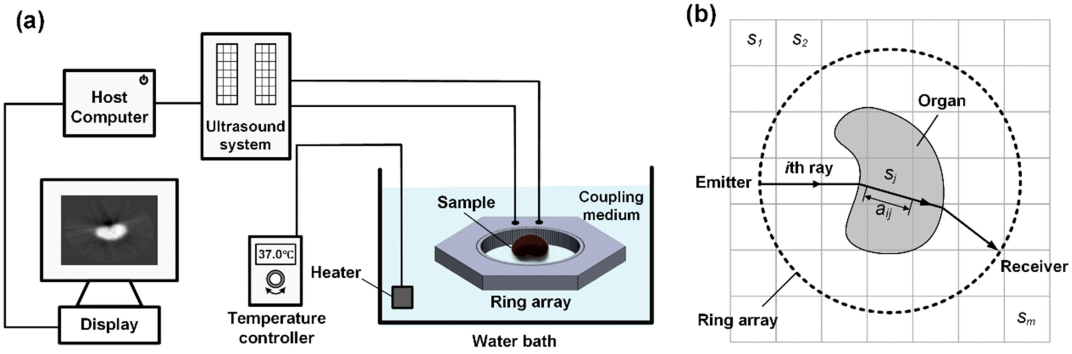


**Fig. 1.** (a) Schematic showing the setup of the USCT imaging system. (b) Principle of bent-ray based image reconstruction. $a_{ij}$ denotes the weight of the ith ray in the jth grid.


DOI: 10.52396/JUSTC-2021-0113
*JUSTC*, **2022**, 52(1): 8

speed images. It is worth noting that to eliminate possible system errors, the travel time of background media is first measured and then subtracted from the travel time data when test samples are present.

All animal experiments were performed in accordance with the NIH Guide for the Care and Use of Laboratory Animals, after approval of the laboratory animal protocol by the Institutional Animal Care and Use Committee (IACUC) of the University of Science and Technology of China (Protocol Number USTCACUC1803065). Twelve adult Sprague-Dawley rats (age: 8~9 weeks, body weight: ~200 g) were used in this study.The rats were euthanized by $CO_2$ inhalation before organs were excised.

# 3 Results

## 3.1 System characterization

The accuracy of the USCT imaging system was calibrated by comparing measurement results of the same samples with those measured by the pulse-echo method proposed by Kuo et al.[30]. In this calibration experiment, gelatin cylinders (Fig.2 a) with mass concentrations varying from 14% to 30% were used as phantoms. Fig.2 b and c show the sound speed image of a 22% gelatin phantom using water at 22 ℃ as the coupling medium and the average sound speed values of the gelatin phantoms at different concentrations by USCT, respectively. The results indicate that the sound speed of the phantom increases with the increase of gelatin concentration. As a comparison, the sound speeds of the gelatin phantoms were also measured by the pulse-echo method. The method employs the same system as USCT but operates the ring array transducer in pulse-echo mode instead of the transmission mode in USCT. Measurement data are presented in Fig.2c in the form of a box plot and tabulated in Table 1 as mean ± standard deviation (SD) for comparison. The results suggest that USCT and the pulse-echo method have comparable measurement accuracy. All samples were measured five times independently in this comparison experiment.

## 3.2 Animal experiments

After the calibration experiment, sound speed imaging and estimation of *ex vivo* organs using USCT were performed. Five types of organs including the brain, heart, liver, spleen, and kidney (the first column of Fig.3) were excised from twelve recently euthanized rats and positioned in the center of the ring array transducer. The freshly excised organs were allowed to stand for two minutes before the imaging procedure starts to ensure temperature equalization between the samples and background PBS buffer. All samples were measured within 20 minutes after excision and the temperature of the PBS buffer was kept at 37 ± 0.2 ℃. The second column of Fig.3 presents the sound speed imaging results, demonstrating that USCT can delineate the shape of the organs based on the sound speed information. To estimate the average sound speed of each organ, masks for the ROIs were generated by thresholding the sound speed maps based on their histograms (Fig.4) and are shown in the third column of Fig.3. Corresponding ROIs within the masks are presented in the last column of Fig.3.

The average sound speed of each type of organ is statistically evaluated within the ROIs and is tabulated in Table 2. The results suggest that the sound speeds measured in this study for the brain, heart, liver, spleen, and kidney are 1560.2 ± 1.8 m·s$^{-1}$, 1579.4 ± 2.1 m·s$^{-1}$, 1591.2 ± 3.3 m·s$^{-1}$, 1574.3 ± 1.2 m·s$^{-1}$, 1575.0 ± 3.5 m·s$^{-1}$, respectively. The liver has the highest sound speed among all five types of organs. The estimated sound speed values were also compared with published data, as shown in Table 3. The measured sound speeds of some organs, e.g., brain and heart, in this study are close to results reported in the literature while the sound speeds of

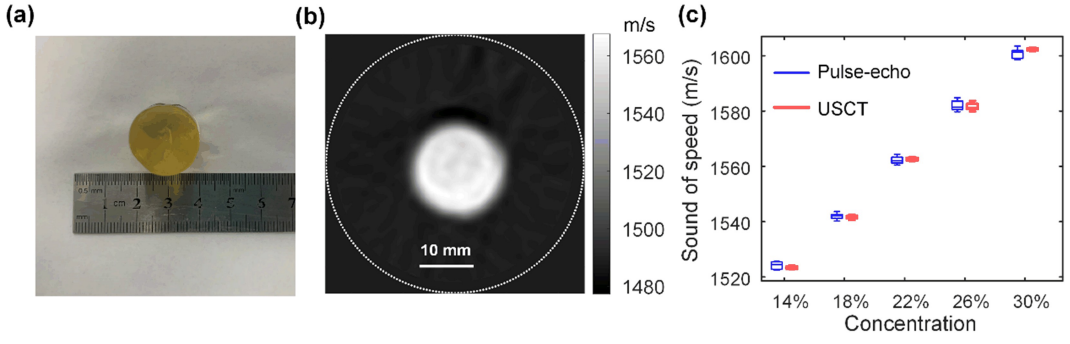


**Fig. 2.** (a) Photograph of a gelatin phantom. (b) Sound speed image of a 22% gelatin phantom. (c) Comparison of average sound speeds of gelatin phantoms at mass concentrations from 14% to 30% measured by USCT and the pulse-echo method.

**Table 1.** Sound speeds of the gelatin phantoms at different concentrations measured by the USCT and the pulse-echo method.

| Concentration | 14% | 18% | 22% | 26% | 30% |
|---|---|---|---|---|---|
| USCT (m·s$^{-1}$)(mean ± SD) | 1523.3 ± 0.3 | 1541.6 ± 0.7 | 1562.6 ± 0.6 | 1581.6 ± 0.2 | 1602.3 ± 0.2 |
| Pulse echo (m·s$^{-1}$)(mean ± SD) | 1524.2 ± 1.4 | 1541.9 ± 1.2 | 1562.2 ± 1.4 | 1582.0 ± 2.0 | 1600.8 ± 1.9 |


DOI: 10.52396/JUSTC-2021-0113
*JUSTC*, **2022**, 52(1): 8

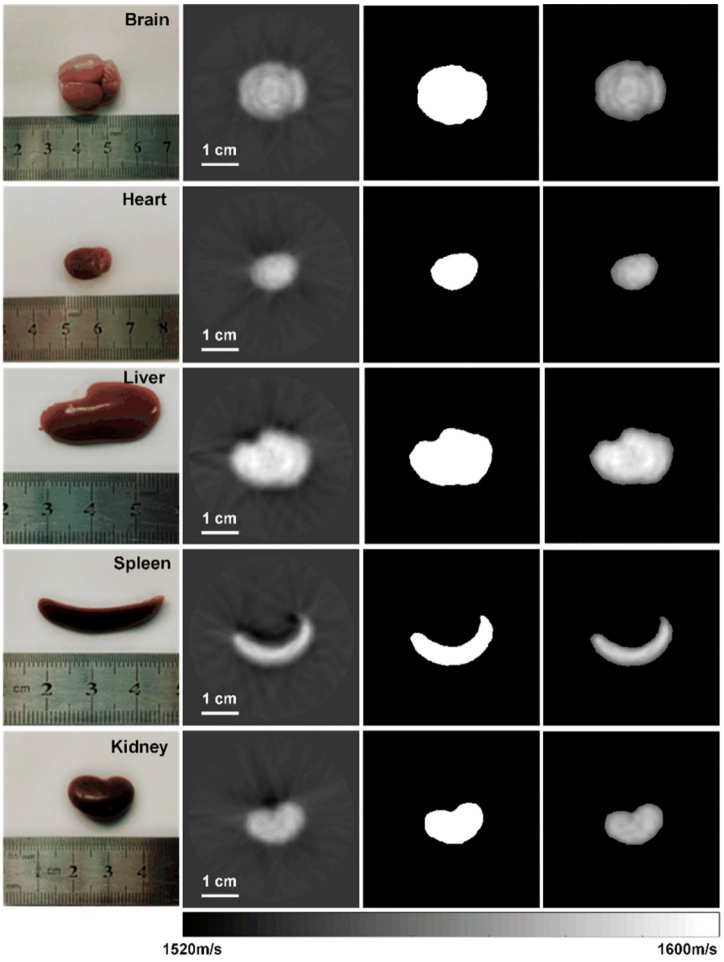


**Fig. 3.** Sound speed maps of rat organs imaged by USCT. First column: photograph of isolated organs. Second column: corresponding sound speed maps. Third column: masks used to segment the regions of interest (ROIs). Fourth column: segmented images used to calculate the average sound speeds. First row to the fifth row: brain, heart, liver, spleen, kidney.

**Table 2.** Average sound speeds of the five types of organs measured by USCT.

| Organ | Brain | Heart | Liver | Spleen | Kidney |
|---|---|---|---|---|---|
| Speed ($m \cdot s^{-1}$)(mean ± SD) | 1560.2 ± 1.8 | 1579.4 ± 2.1 | 1591.2 ± 3.3 | 1574.3 ± 1.2 | 1575.0 ± 3.5 |

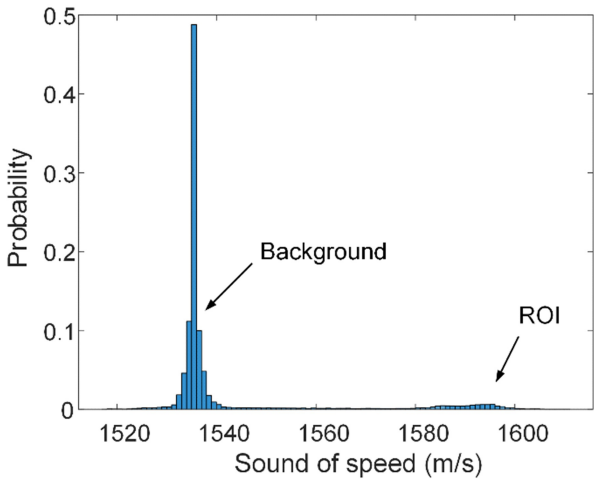


**Fig. 4.** Histogram of a typical sound speed image. The histogram has two peaks. One peak represents the background (PBS buffer) and the other indicates the ROI.

others, such as liver and spleen, slightly deviate from previously published results. This is probably due to the differences in measurement procedures of different methods. The USCT method proposed in this study can measure the sound speeds of animal whole organs immediately after excision. Moreover, it is a global measurement method, which indicates that the estimated sound speed is an average representation of the sound speed of a whole organ. In contrast, most measurement methods used in the literature require complicated sample preparation procedures and can only reflect the local sound speed property of an organ. Therefore, measured sound speed may vary at different organ locations due to tissue heterogeneity.

## 4 Conclusions

In conclusion, we developed a USCT technique based on a ring array transducer for sound speed imaging and evaluation of small animal organs *ex vivo*. The proposed technique can


DOI: 10.52396/JUSTC-2021-0113
*JUSTC*, **2022**, 52(1): 8

**Table 3.** Comparison of measured sound speeds of the five types of organs in this study with published data.

| Organ | Temperature (℃) | Frequency (MHz) | Speed ($m \cdot s^{-1}$) (mean ± SD) | Species | Reference |
|---|---|---|---|---|---|
| Brain | 37 | 1-5 | 1562 | Human,*in vitro* | [31] |
| | 37.2 | 12-32 | 1566.3 ± 9.9 | Mouse, *ex vivo* | [32] |
| | 37 | 3 | 1560.2 ± 1.8 | Rat, *ex vivo* | This study |
| Heart | 37 | 3.5 | 1580 | Rat, *in vitro* | [33] |
| | 37 | 3 | 1579.4 ± 2.1 | Rat, *ex vivo* | This study |
| | 37 | 3 | 1578.3 ± 5.4 | Human, *in vivo* | [34] |
| | 37.2 | NA[a] | 1578.1 ± 2.9 | Human, *ex vivo* | [24] |
| | 37 | 1-7 | 1607 | Human, *ex vivo* | [35] |
| | 20 | 1-6 | 1577 ± 11 | Human, *ex vivo* | [6] |
| | 37 | 2.25 | 1592 ± 6 | Human, *ex vivo* | [36] |
| Liver | 37 | 3.5 | 1605.1 ± 3.2 | Rat, *ex vivo* | [2] |
| | 36.3 | 7 | 1596.6 ± 4.8 | Rat, *ex vivo* | [37] |
| | 23 | 80 | 1598 - 1677 | Rat, *in vitro* | [21] |
| | 23 | 250 | 1568 - 1668 | Rat, *in vitro* | [21] |
| | 37.2 | 12-32 | 1604.7 ± 16.8 | Mouse,*ex vivo* | [32] |
| | 37 | 3 | 1591.2 ± 3.3 | Rat, *ex vivo* | This study |
| | 37 | 3 | 1567 ± 8.5 | Human, *in vivo* | [34] |
| Spleen | 37.2 | NA | 1567 ± 2.3 | Human, *ex vivo* | [24] |
| | 37 | 3 | 1574.3 ± 1.2 | Rat, *ex vivo* | This study |
| | 37.2 | NA | 1560.2 ± 1.8 | Human, *ex vivo* | [24] |
| Kidney | 23-26 | 100 | 1586 ± 10.7 | Mouse, *ex vivo* | [38] |
| | 37.2 | 12-32 | 1574.9 ± 10.8 | Mouse, *ex vivo* | [32] |
| | 37 | 3 | 1575.0 ± 3.5 | Rat, *ex vivo* | This study |

[Note] [a]NA: not available.

not only measure average sound speed values of soft tissues but also provide two-dimensional cross-sectional sound speed images. It does not need complicated sample preparation procedures and can yield accurate measurement results. The measured sound speeds of the brain, heart, liver, spleen, and kidney are close to published data and can be used as a reference for disease diagnosis and image quality optimization in photoacoustic tomography. This work demonstrates a new method for sound speed imaging and evaluation of soft tissues and can potentially be extended to *in vivo* applications.

## Acknowledgments

The work is supported by the Anhui Provincial Department of Science and Technology(18030801138), the National Natural Science Foundation of China(61705216, 12174368, 62122072), the Zhejiang Lab(2019MC0AB01).

## Conflict of interest

The authors declare that they have no conflict of interest.

## Biographies

**Zhiming Hu** is a graduate student under the supervision of Prof. Chao Tian at the University of Science and Technology of China (USTC). His current research is focused on ultrasound computed tomography.

**Chao Tian** is a professor at the School of Engineering Science, University of Science and Technology of China (USTC). He received the B.S. degree in Electrical Engineering and the PhD degree in Optical Engineering from Zhejiang University, Hangzhou, China. From 2013 to 2017, he worked as a Post-Doctoral Research Fellow in photo-acoustic imaging with the Department of Biomedical Engineering at the University of Michigan, Ann Arbor. He has published over 40 peer-reviewed journal articles and is a co-inventor of six patents. Dr. Tian is a Senior Member of OSA and a member of SPIE and IEEE. His research interests focus on photo-acoustic and ultrasound imaging and their biomedical applications.

## References

[1] Duck F A. Physical Properties of Tissues: a Comprehensive Reference Book. Academic Press, 1990. https://sciencedirect.53yu.com/book/9780122228001/physical-properties-of-tissues.

[2] Hachiya H, Ohtsuki S, Tanaka M. Relationship between speed of sound in and density of normal and diseased rat livers. *Japanese Journal of Applied Physics,* **1994**, *33* (5S): 3130.

[3] Ghoshal G, Lavarello R J, Kemmerer J P, et al. Ex vivo study of quantitative ultrasound parameters in fatty rabbit livers. *Ultrasound in Medicine and Biology,* **2012**, *38* (12): 2238–2248.

[4] Wiskin J, Malik B, Natesan R, et al. Quantitative assessment of breast density using transmission ultrasound tomography. *Medical Physics,* **2019**, *46* (6): 2610–2620.

[5] Zografos G, Liakou P, Koulocheri D, et al. Differentiation of BIRADS-4 small breast lesions via multimodal ultrasound tomography. *European Radiology,* **2015**, *25* (2): 410–418.



DOI: 10.52396/JUSTC-2021-0113
*JUSTC*, **2022**, 52(1): 8

[6] Bamber J C, Hill C R. Acoustic properties of normal and cancerous human liverjI. Dependence on pathological condition. *Ultrasound in Medicine and Biology,* **1981**, *7* (2): 121–133.
[7] Li C, Duric N, Littrup P, et al. In Vivo breast sound-speed imaging with ultrasound tomography. *Ultrasound in Medicine and Biology,* **2009**, *35* (10): 1615–1628.
[8] Ruiter N V, Zapf M, Hopp T, et al. 3D ultrasound computer tomography of the breast: A new era? *European Journal of Radiology,* **2012**, *81* (S): 133–134.
[9] Ding M, Song J, Zhou L, et al. In Vitro and in Vivo evaluations of breast ultrasound tomography imaging system in HUST. Medical Imaging 2018 ——4th World Congress on Medical Imaging and Clinical Research. London: International Society for Optics and Photonics, 2018: 105800P. https://www.spiedigitallibrary.org/conference-proceedings-of-spie/10580/105800P/In-vitro-and-in-vivo-evaluations-of-breast-ultrasound-tomography/10.1117/12.2292985.short.
[10] Anderson M E, McKeag M S, Trahey G E. The impact of sound speed errors on medical ultrasound imaging. *The Journal of the Acoustical Society of America,* **2000**, *107* (6): 3540–3548.
[11] Tian C, Zhang C, Zhang H, et al. Spatial resolution in photoacoustic computed tomography. *Reports on Progress in Physics,* **2021**, *84* (3): 036701.
[12] Wang T, Liu W, Tian C. Combating acoustic heterogeneity in photoacoustic computed tomography: A review. *Journal of Innovative Optical Health Sciences,* **2020**, *13* (03): 2030007.
[13] Feng T, Zhu Y, Morris R, et al. Functional photoacoustic and ultrasonic assessment of osteoporosis: A clinical feasibility study. *BME Frontiers,* **2020**, *2020*: 1081540.
[14] Ophir J. Estimation of the speed of ultrasound propagation in biological tissues: A beam-tracking method. *IEEE Transactions on Ultrasonics, Ferroelectrics, and Frequency Control,* **1986**, *33* (4): 359–368.
[15] Ophir J, Moriya T, Yazdi Y. A single transducer transaxial compression technique for the estimation of sound speed in biological tissues. *Ultrasonic Imaging,* **1991**, *13* (3): 269–279.
[16] Yoon C, Lee Y, Chang J H, et al. In Vitro estimation of mean sound speed based on minimum average phase variance in medical ultrasound imaging. *Ultrasonics,* **2011**, *51* (7): 795–802.
[17] Jakovljevic M, Hsieh S, Ali R, et al. Local speed of sound estimation in tissue using pulse-echo ultrasound: Model-based approach. *The Journal of the Acoustical Society of America,* **2018**, *144* (1): 254–266.
[18] Kondo M, Takamizawa K, Hirama M, et al. An evaluation of an in vivo local sound speed estimation technique by the crossed beam method. *Ultrasound in Medicine and Biology,* **1990**, *16* (1): 65–72.
[19] Byram B C, Trahey G E, Jensen J A. A method for direct localized sound speed estimates using registered virtual detectors. *Ultrasonic Imaging,* **2012**, *34* (3): 159–180.
[20] Robinson D E, Ophir J, Wilson L S, et al. Pulse-echo ultrasound speed measurements: progress and prospects. *Ultrasound in Medicine and Biology,* **1991**, *17* (6): 633–646.
[21] Irie S, Inoue K, Yoshida K, et al. Speed of sound in diseased liver observed by scanning acoustic microscopy with 80 MHz and 250 MHz. *The Journal of the Acoustical Society of America,* **2016**, *139* (1): 512–519.
[22] Greenleaf J F, Johnson S A, Lee S L, et al. Algebraic reconstruction of spatial distributions of acoustic absorption within tissue from their two-dimensional acoustic projections. *Acoustical Holography: Springer,* **1974**: 591–603.
[23] PÁrez-Liva M, Herraiz J L, UdÕas J M, et al. Time domain reconstruction of sound speed and attenuation in ultrasound computed tomography using full wave inversion. *The Journal of the Acoustical Society of America,* **2017**, *141* (3): 1595–1604.
[24] Rajagopalan B, Greenleaf J F, Thomas P J, et al. Variation of acoustic speed with temperature in various excised human tissues studied by ultrasound computerized tomography. The Second International Symposium on Ultrasonic Tissue Characterization, (US Department of Commerce, National Bureau of Standards, 1979: 227. https://xs.dailyheadlines.cc/books?hl=zh-CN&lr&idAL7AirGJZfkC&oifnd&pgPA227&otsR-lsIWQxtU&signEvwV5cHatxexxkatqdUEu0c-Fw.
[25] Del Grosso V A, Mader C W. Speed of sound in pure water. *The Journal of the Acoustical Society of America,* **1972**, *52* (5B): 1442–1446.
[26] Coppens A B. Simple equations for the speed of sound in Neptunian waters. *The Journal of the Acoustical Society of America,* **1981**, *69* (3): 862–863.
[27] Li C, Huang L, Duric N, et al. An improved automatic time-of-flight picker for medical ultrasound tomography. *Ultrasonics,* **2009**, *49* (1): 61–72.
[28] Ali R, Hsieh S, Dahl J. Open-source Gauss-Newton-based methods for refraction-corrected ultrasound computed tomography. Medical Imaging 2019, International Society for Optics and Photonics. London: SPIE, 2019: 1095508. https://www.spiedigitallibrary.org/conference-proceedings-of-spie/10955/1095508/Open-source-Gauss-Newton-based-methods-for-refraction-corrected-ultrasound/10.1117/12.2511319.short?sessionGUID=329ad883-c9d9-02bc-9993-ced268bead49&sessionUID=329ad883-c9d9-02bc-9993-ced268bead49&webSyncD=c89a0ce4-6e9e-6ec7-a49d-ab6a0cbad059.
[29] Aster R C, Borchers B, Thurber C H. Parameter Estimation and Inverse Problems. 3ed, Elsevier, 2018: 165. http://www.ees.nmt.edu/outside/courses/GEOP529/Docs/old/preface.pdf.
[30] Kuo I Y, Hete B, Shung K K. A novel method for the measurement of acoustic speed. *The Journal of the Acoustical Society of America,* **1990**, *88* (4): 1679–1682.
[31] Kremkau F W, Barnes R W, McGraw C P. Ultrasonic attenuation and propagation speed in normal human brain. *The Journal of the Acoustical Society of America,* **1981**, *70* (1): 29–38.
[32] Rabell-Montiel A, Thomson A J, Anderson T A, et al. Acoustic properties of small animal soft tissue in the frequency range 12~32 MHz. *Ultrasound in Medicine and Biology,* **2018**, *44* (3): 702–713.
[33] Hachiya H, Ohtsuki S. Non-contact measurement of sound speed of tissues. *Ultrasonic Tissue Characterization, Springer,* **1996**: 63–72.
[34] Chen C F, Robinson D E, Wilson L S, et al. Clinical sound speed measurement in liver and spleen in Vivo. *Ultrasonic Imaging,* **1987**, *9* (4): 221–235.
[35] Bamber J C, Hill C R. Ultrasonic attenuation and propagation speed in mammalian tissues as a function of temperature. *Ultrasound in Medicine and Biology,* **1979**, *5* (2): 149–157.
[36] Sehgal C M, Brown G M, Bahn R C, et al. Measurement and use of acoustic nonlinearity and sound speed to estimate composition of excised livers. *Ultrasound in Medicine and Biology,* **1986**, *12* (11): 865–874.
[37] Kumagai H, Yokoyama K, Katsuyama K, et al. A new method for measuring the speed of sound in rat liver ex vivo using an ultrasound system: Correlation of sound speed with fat deposition. *Ultrasound in Medicine and Biology,* **2014**, *40* (10): 2499–2507.
[38] Frizzell L A, Gindorf J D. Measurement of ultrasonic velocity in several biological tissues. *Ultrasound in Medicine & Biology,* **1981**, *7* (4): 385–387.


DOI: 10.52396/JUSTC-2021-0113
*JUSTC*, **2022**, 52(1): 8